Evidence for thermally activated delayed fluorescence in iridium(III) complexes

P. Pander,[a,b*] D. Nastula,[a] P. H. Marek-Urban,[a,b,c] V. N. Kozhevnikov,[d] and J. A. Gareth Williams[e]

E-mail: piotr.pander@polsl.pl

[a] *Faculty of Chemistry, Silesian University of Technology, M. Strzody 9, 44-100 Gliwice, Poland.*
[b] *Centre for Organic and Nanohybrid Electronics, Silesian University of Technology, Konarskiego 22B, 44-100 Gliwice, Poland.*
[c] *Faculty of Chemistry, Warsaw University of Technology, Noakowskiego 3, 00-664 Warsaw, Poland.*
[d] *Department of Applied Sciences, Faculty of Health and Life Sciences, Northumbria University, Newcastle Upon Tyne, Tyne and Wear, NE1 8ST, United Kingdom.*
[e] *Department of Chemistry, Durham University, South Road, Durham, DH1 3LE, United Kingdom.*

Table of contents

1. General

Extraction of experimental data from figures in published sources

Experimental data reported in earlier works were obtained from the respective figures included within the main text or the ESI of the said publications. Highest resolution graphics were used, where available. We used WebPlotDigitizer software, available from https://automeris.io/, to extract the experimental data from graphics into an ASCII format. Data sources have been acknowledged where the respective data is being used in the main text of this work.

Theory

We use density functional theory (DFT) and time-dependent DFT (TD-DFT) as well as the quasi-degenerate perturbation theory (QDPT)[1,2] with zeroth-order regular approximation (ZORA)[3,4] implemented in Orca 5.0.3[5,6] in order to gain insights into the luminescence mechanisms in the studied iridium(III) complexes. Ground state (S_0) and triplet excited state (T_1) geometries were optimised at the BP86/def2-TZVP[7] level of theory which was found to be the most optimal for this task. We used def2/J[8] auxiliary basis set and atom-pairwise dispersion correction with the Becke-Johnson damping scheme (D3BJ)[9,10]. All optimisations were performed with tight SCF and geometry convergence criteria. Excited state energy of TD-DFT states was calculated using the resultant T_1 geometry at the B3LYP/def2-TZVP[7] level of theory using CPCM for the appropriate solvent. In this case relativistically corrected triple-zeta basis sets with the zeroth-order regular approximation (ZORA)[3,4] were used: ZORA-def2-TZVP[7] with the SARC/J[11] auxiliary basis for all atoms except Ir and I for which a segmented all-electron relativistically contracted (SARC) SARC-ZORA-TZVP[11] basis set was used. Spin-orbit coupling (SOC) calculations were performed as implemented in the ORCA software. SOC matrix elements (SOCME) and SOC-corrected excitations (SOC states) were computed using the same settings. The RI-SOMF(1X) setting was used to accelerate SOC calculations. These settings have previously been used to model an earlier example of a TADF di-Ir(III) complex[28] and has shown a perfect agreement of the computational model with experiment with the experiment. All molecular orbital (MO) iso surfaces were visualised using Gabedit 2.5.0.[12]

Calculation of singlet and triplet radiative rates using simulated parameters

Relationship between transition oscillator strength and radiative rate is described by[14]:

$$k_r = \frac{n^2 \nu^2 f}{1.5}$$

Where k_r – radiative rate of a given transition, s^{-1}; n – refractive index of the medium; ν – energy of the state, cm^{-1}; f – transition oscillator strength.

In order to obtain radiative decay rates involving 1,2,3…n SOC states we consider the thermal equilibrium between them as set out earlier by Mori and others[15] for calculating phosphorescence rates:

$$k_r^{1-3} = \frac{k_r^1 + k_r^2 e^{-\frac{\Delta E_{1,2}}{k_B T}} + k_r^3 e^{-\frac{\Delta E_{1,3}}{k_B T}}}{1 + e^{-\frac{\Delta E_{1,2}}{k_B T}} + e^{-\frac{\Delta E_{1,3}}{k_B T}}}$$

$$k_r^{1-n} = \frac{k_r^1 + \sum_2^n \left(k_r^n e^{-\frac{\Delta E_{1,n}}{k_B T}} \right)}{1 + \sum_2^n \left(e^{-\frac{\Delta E_{1,n}}{k_B T}} \right)}$$

Where: k_r^{1-3} – average T_1 radiative rate, s^{-1}; k_r^{1-n} – average radiative rate involving excited SOC states 1 to n, s^{-1}; k_r^1, k_r^2, k_r^3, k_r^n – radiative rates of the SOC-TDDFT states 1-3 and n, s^{-1}; k_B – Boltzmann constant, 8.617×10^{-5} eV K^{-1}; $\Delta E_{1,2}$ – energy difference between SOC-TDDFT states 1 and 2, eV; $\Delta E_{1,3}$ – energy difference between SOC-TDDFT states 1 and 3, eV; $\Delta E_{1,n}$ – energy difference between SOC-TDDFT states 1 and n, eV; T – temperature, K.

For the purpose of this work we assume T = 295 K unless stated otherwise.

Exemplar calculation for triplet radiative rates using complex 6-B1

Orca outputs for the T_1 geometry of **6-B1** are collected in the table below.

SOC state	**State assignment**	**State energy ν, cm^{-1}**	**State energy E, eV**	**f_{osc}**
1	T_1	17292	2.1439	3.62×10^{-4}
2	T_1	17326	2.1480	3.25×10^{-4}
3	T_1	17534	2.1739	1.07×10^{-2}
4	S_1	17632	2.1861	2.79×10^{-2}

We first calculate the k_r values according to the equation described in the preceding section:

$$k_r = \frac{n^2 \nu^2 f}{1.5}$$

We use refractive index n = 1.4241 for dichloromethane, hence:

$$k_r^1 = \frac{1.4241^2 \cdot 17292^2 \cdot 3.62 \cdot 10^{-4}}{1.5} = 1.46 \cdot 10^5 s^{-1}$$

$$k_r^2 = \frac{1.4241^2 \cdot 17326^2 \cdot 3.25 \cdot 10^{-4}}{1.5} = 1.32 \cdot 10^5 s^{-1}$$

$$k_r^3 = \frac{1.4241^2 \cdot 17534^2 \cdot 1.07 \cdot 10^{-2}}{1.5} = 4.45 \cdot 10^6 s^{-1}$$

$$k_r^4 = \frac{1.4241^2 \cdot 17632^2 \cdot 2.79 \cdot 10^{-2}}{1.5} = 1.17 \cdot 10^7 s^{-1}$$

Boltzmann constant $k_B = 8.617 \times 10^{-5}$ eV K^{-1}. From the above the k_r^1 to k_r^3 are the radiative decay rate constants of the three T_1 sublevels and hence the cumulative T_1 radiative decay rate at T = 295 K is:

$$k_r^{1-3} = \frac{1.46 \cdot 10^5 + 1.32 \cdot 10^5 \cdot e^{-\frac{2.1480-2.1439}{8.617 \cdot 10^{-5} \cdot 295}} + 4.45 \cdot 10^6 \cdot e^{-\frac{2.1739-2.1439}{8.617 \cdot 10^{-5} \cdot 295}}}{1 + e^{-\frac{2.1480-2.1439}{8.617 \cdot 10^{-5} \cdot 295}} + e^{-\frac{2.1739-2.1439}{8.617 \cdot 10^{-5} \cdot 295}}} = 7.54 \cdot 10^5 s^{-1}$$

k_r^4 is the S_1 radiative decay rate constant, hence $k_r^S = k_r^4$

The radiative decay rate *constant* including T_1 decay rate and TADF at T = 295 K is:

$$k_r^{1-3} = \frac{1.46 \cdot 10^5 + 1.32 \cdot 10^5 \cdot e^{-\frac{2.1480-2.1439}{8.617 \cdot 10^{-5} \cdot 295}} + 4.45 \cdot 10^6 \cdot e^{-\frac{2.1739-2.1439}{8.617 \cdot 10^{-5} \cdot 295}} + 1.17 \cdot 10^7 \cdot e^{-\frac{2.1861-2.1439}{8.617 \cdot 10^{-5} \cdot 295}}}{1 + e^{-\frac{2.1480-2.1439}{8.617 \cdot 10^{-5} \cdot 295}} + e^{-\frac{2.1739-2.1439}{8.617 \cdot 10^{-5} \cdot 295}} + e^{-\frac{2.1861-2.1439}{8.617 \cdot 10^{-5} \cdot 295}}} = 1.64 \cdot 10^6 s^{-1}$$

Equipment and methods for photophysical measurements

Photoluminescence measurements of **6-A1** were conducted in toluene solution degassed with three freeze-pump cycles. Thin films in polystyrene (M_w = 300 000) were deposited from chloroform solutions. The films were fabricated by spin-coating and dried under vacuum at room temperature. Absorption spectra in solution were recorded with an Evolution One Plus (Thermo Fisher Scientific) double beam spectrophotometer. Photoluminescence (PL) spectra in solution and film were recorded using an FS5 Edinburgh Instruments spectrofluorometer or a QePro (Ocean Optics) spectrometer. PLQY in film was obtained using an integrating sphere integrated with the FS5 apparatus. Photoluminescence decays in film were recorded using nanosecond gated luminescence and lifetime measurements (from 1 ns to 1 s) using the third harmonic (355 nm) of a high-energy pulsed Nd:YAG laser Q-SPARK-A50-TH-RE (Quantum Light Instruments). The emitted light was focused onto a spectrograph and detected with a sensitive gated iCCD camera (Stanford Computer Optics). Time-resolved measurements were performed by exponentially increasing gate and integration times.

Further details are available in an earlier work.[1] Temperature-dependent experiments were conducted using a cryocooler and a cold head (Lakeshore) at vacuum.

OLED devices

OLEDs were fabricated by spin-coating / evaporation hybrid method. The hole injection layer (PEDOT AI4083), hole transport layer PVKH, and emitting layer (mCP:PO-T2T + dopant, mCP:PBD + dopant) were spin-coated, whereas the electron transport layer (PO-T2T or TmPyPB) and cathode (LiF/Al) were evaporated. The devices were of 4×2 mm pixel size. 2,4,6-Tris[3-(diphenylphosphinyl)phenyl]-1,3,5-triazine (PO-T2T, LUMTEC), 1,3-bis(carbazol-9-yl)benzene (mCP, sublimed, LUMTEC), 2-(4-biphenyl)-5-(4-*tert*-butylphenyl)-1,3,4-oxadiazole (PBD, Sigma Aldrich), poly(*N*-vinylcarbazole) (PVKH, Sigma Aldrich, M = 10^6 Da), 1,3,5-tri[(3-pyridyl)-phen-3-yl]benzene (TmPyPB, Lumtec), LiF (99.995%, Sigma Aldrich), and aluminium pellets (99.9995%, Lesker) were purchased from the companies indicated in the parentheses. Pre-patterned indium-tin-oxide (ITO) on glass substrate was used, with a sheet resistance of 20 Ω/sq and ITO thickness of 100 nm. The substrates were cleaned by sonicating in acetone and subsequently in isopropanol for 15 minutes each and then treated with oxygen plasma for 6 minutes at full power. PEDOT AI4083 was spin-coated and annealed on a hotplate at 120 ˚C for 15 min to give a 30 nm film. 10 nm PVKH layer was obtained from a 3 mg mL^{-1} solution in chloroform:chlorobenzene (95:5 v/v). The emitting layer was deposited from a toluene solution (10 mg mL^{-1} total solids content) for mCP:PO-T2T and mCP:PBD hosts. The dopant was dissolved in the solution of blend host in order to obtain the final 1% or 3% concentration in the emitting layer. All solutions were filtered directly before use with a PVDF (organic solvents) and PES (PEDOT AI4083) syringe filter with 0.45 μm pore size. All other layers were thermally evaporated using Kurt J. Lesker Super Spectros deposition system at 10^{-8} mbar base pressure and a LC Technology Solutions glovebox. All organic materials and aluminium were deposited at a rate of 1 Å s^{-1}. The LiF layer was deposited at a rate of 0.1–0.2 Å s^{-1}. Characterisation of OLED devices was conducted in a 10 inch integrating sphere (Labsphere) connected to a Keithley 2400 Source Measure Unit and coupled with a QePRO (Ocean Optics) spectrometer. Further details are available in earlier work.[5]

2. Photophysics

Table S1. Experimental photophysical characteristics of the studied iridium(III) complexes at RT.

Complex	**Solvent**	**λ_{PL}, nm**	**PLQY**	**τ, µs**	**k_r, 10^6 s^{-1}**
1-*rac*	CH_2Cl_2	626	0.65	0.76	0.86
1-*meso*	CH_2Cl_2	626	0.65	0.73	0.89
2-5	toluene	559	0.9	1.16	0.78
2-6	toluene	575	0.95	0.44	2.16
3-Ir_2I_2	toluene	585	0.9	0.34	2.65
4-CNIr	THF	695	0.16	0.14	1.14
4-TCNIr	THF	708	0.06	0.15	0.40
5-3	toluene	538	0.15	1.00	0.15
5-5	toluene	643	0.8	1.31	0.61
6-A1	CH_2Cl_2	552	0.94	0.44	2.14
6-A2	CH_2Cl_2	567	0.88	0.57	1.54
6-A3	CH_2Cl_2	568	0.91	0.59	1.54
6-A4	CH_2Cl_2	528	1	0.36	2.78
6-A5	CH_2Cl_2	573	0.94	4.00	0.24
6-B1	CH_2Cl_2	543	1	0.55	1.82
6-C1	CH_2Cl_2	525	1	0.59	1.69
7-B1	CH_2Cl_2	460	0.78	0.63	1.23
7-B2	CH_2Cl_2	464	0.75	0.65	1.16
7-B3	CH_2Cl_2	462	0.83	0.61	1.37

Table S2. Transition oscillator strength and radiative decay rate obtained from the lowest absorption band using the Strickler-Berg method, assuming triplet and singlet nature of the absorption band.

Complex	Solvent	ν_{PL}, cm^{-1}	Triplet absorption		Singlet absorption	
			f_{osc}^{SB}	${}^{SB}k_r^T$, $10^6\ s^{-1}$	f_{osc}^{SB}	${}^{SB}k_r^S$, $10^6\ s^{-1}$
1-*rac**	CH_2Cl_2	15974	0.0130	4.47	0.0389	13.40
1-*meso**	CH_2Cl_2	15974	0.0130	4.47	0.0389	13.40
2-5	toluene	17889	0.0046	2.19	0.0138	6.58
2-6	toluene	17391	0.0152	6.86	0.0455	20.57
3-Ir_2I_2	toluene	17094	0.0120	5.22	0.0359	15.67
4-CNIr	THF	14388	0.0022	0.59	0.0065	1.77
4-TCNIr	THF	14124	0.0010	0.27	0.0031	0.82
5-3	toluene	18587	0.0138	7.13	0.0414	21.38
5-5	toluene	15552	0.0539	19.49	0.1618	58.46
6-A1	CH_2Cl_2	18116	0.0121	5.38	0.0364	16.15
6-A2	CH_2Cl_2	17637	0.0106	4.45	0.0318	13.36
6-A3	CH_2Cl_2	17606	0.0137	5.75	0.0411	17.24
6-A4	CH_2Cl_2	18939	0.0111	5.38	0.0333	16.15
6-A5	CH_2Cl_2	17452	0.0205	8.43	0.0614	25.30
6-B1	CH_2Cl_2	18416	0.0115	5.25	0.0344	15.76
6-C1	CH_2Cl_2	19048	0.0092	4.53	0.0277	13.60
7-B1	CH_2Cl_2	21739	0.0041	2.60	0.0122	7.80
7-B2	CH_2Cl_2	21552	0.0023	1.46	0.0070	4.39
7-B3	CH_2Cl_2	21645	0.0052	3.28	0.0155	9.83

3. Theory

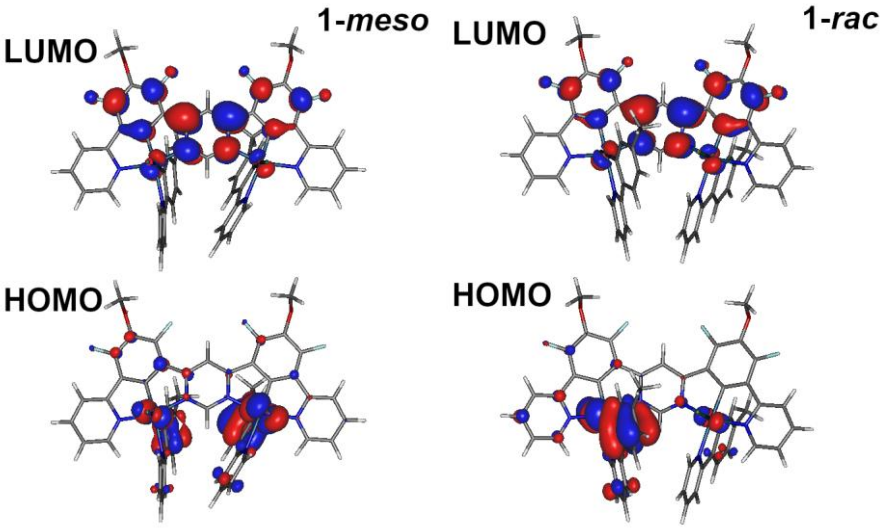

Figure S1. Molecular orbitals involved in the S_1 and T_1 states in complexes **1-*meso*** and **1-*rac***.

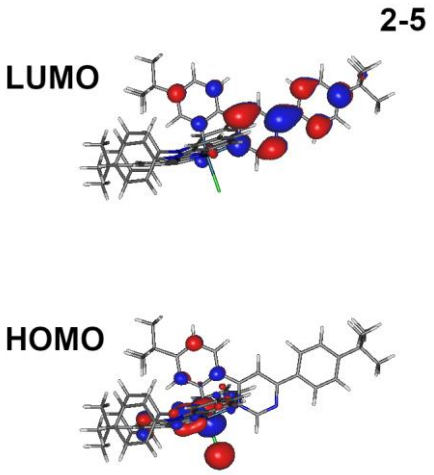

Figure S2. Molecular orbitals involved in the S_1 and T_1 states in complex **2-5**.

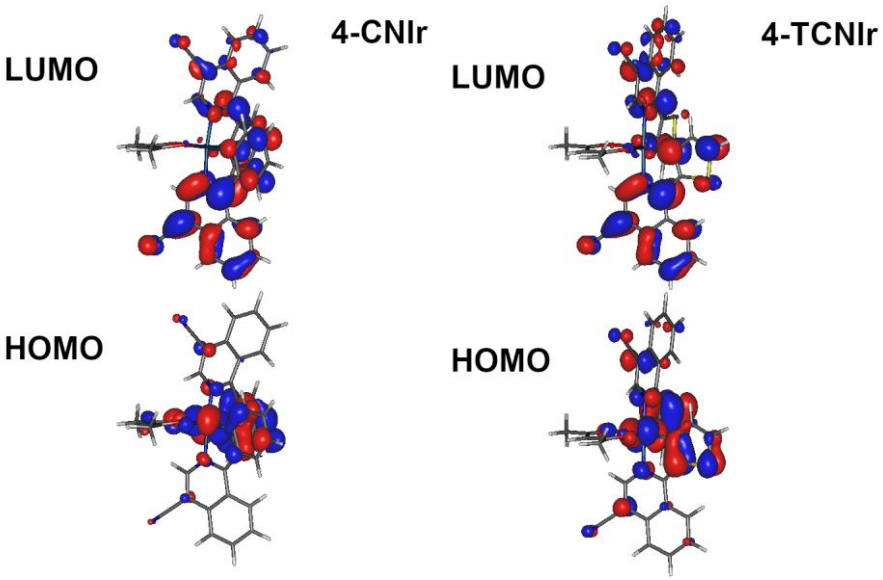

Figure S3. Molecular orbitals involved in the S_1 and T_1 states in complexes **4-CNIr** and **4-TCNIr**.

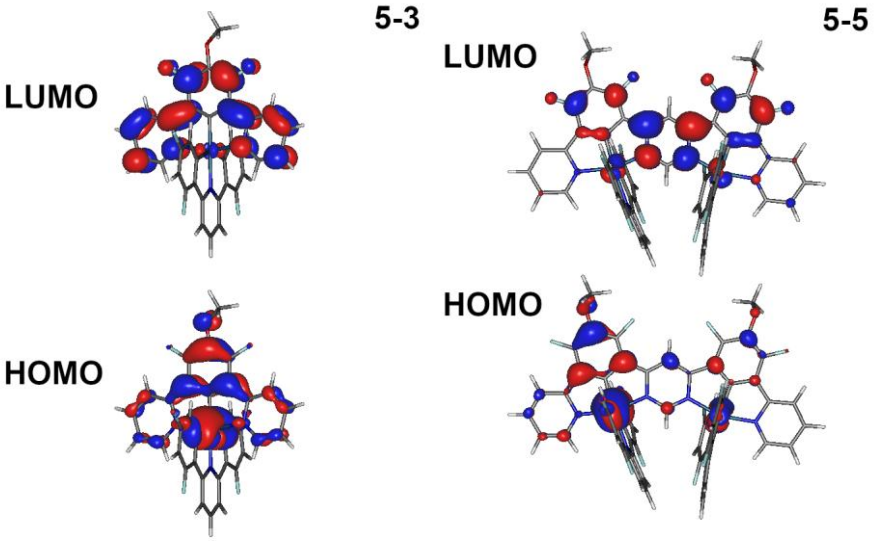

Figure S4. Molecular orbitals involved in the S_1 and T_1 states in complexes **5-3** and **5-5**.

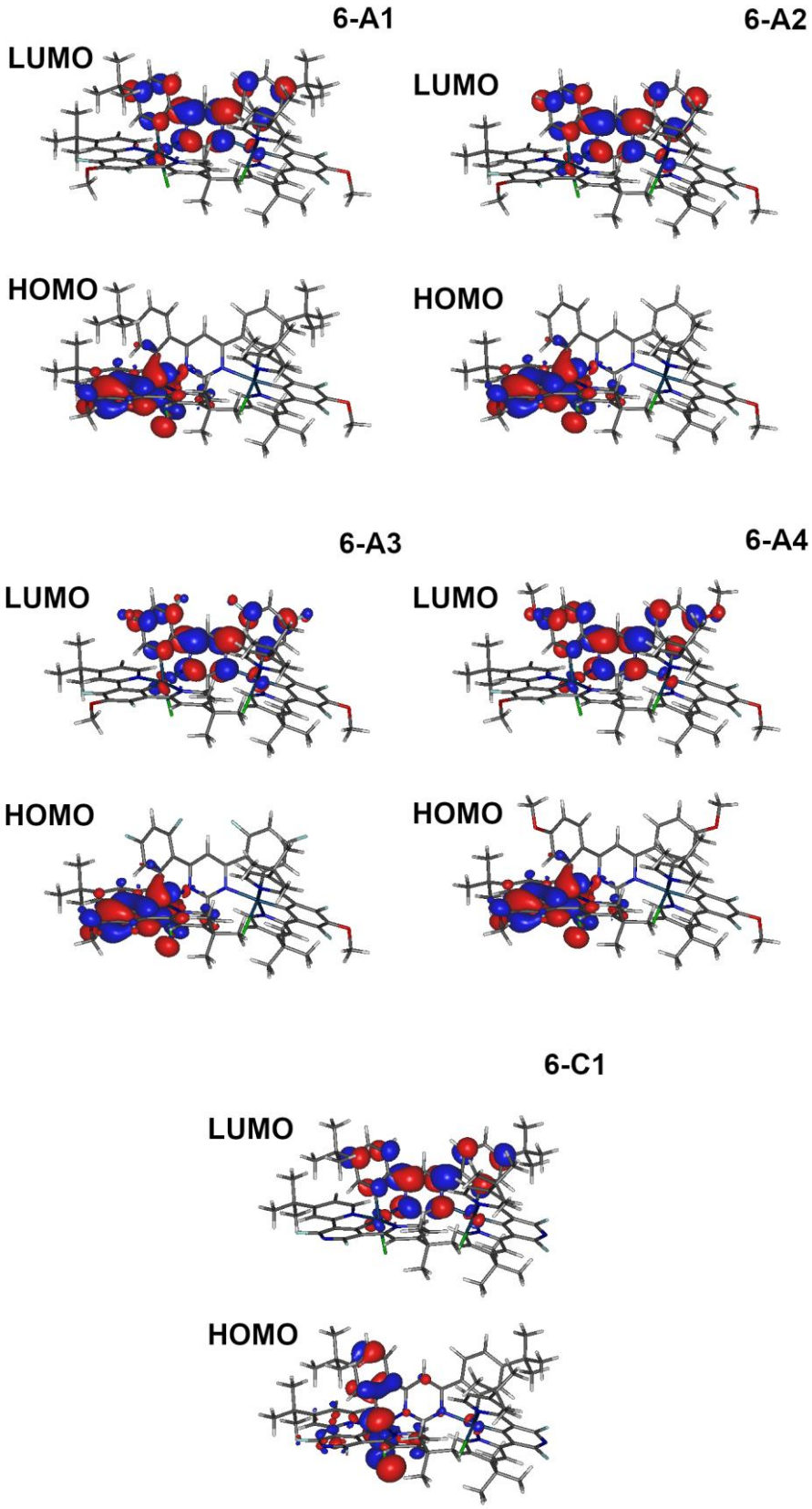

Figure S5. Molecular orbitals involved in the S_1 and T_1 states in complexes **6-A1**, **6-A2**, **6-A3**, **6-A4** and **6-C1**.

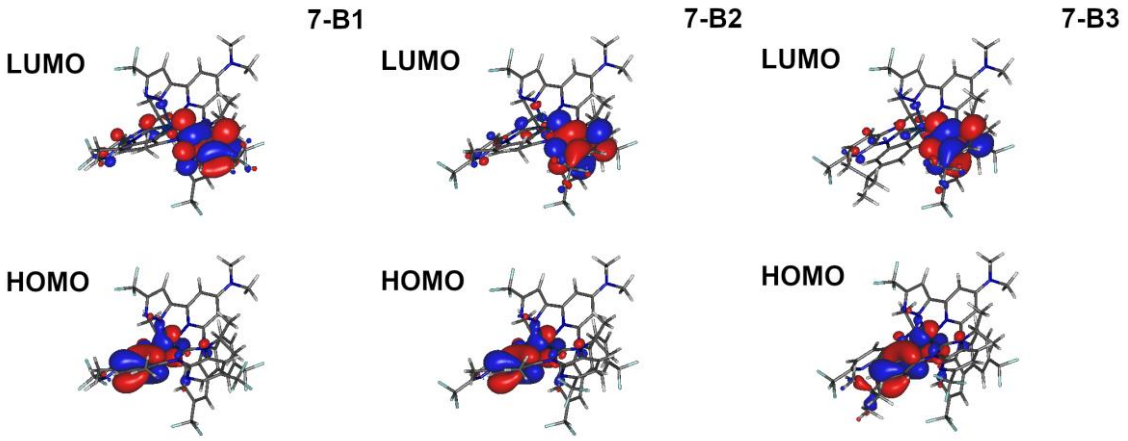

Figure S6. Molecular orbitals involved in the S_1 and T_1 states in complexes **7-B1**, **7-B2** and **7-B3**.

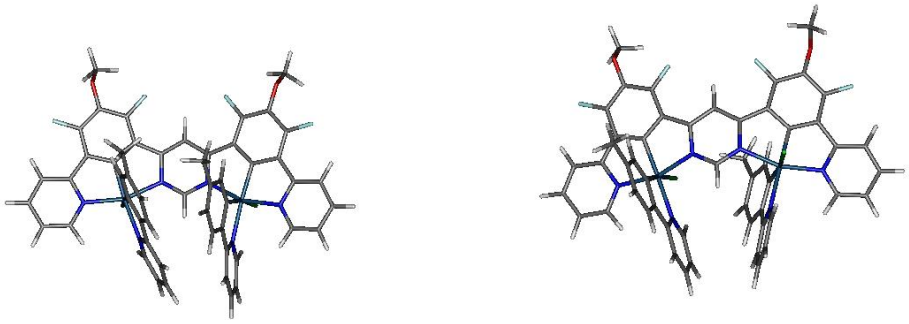

Figure S7. Structural geometry of **1-rac** (*left*) and **1-meso** (*right*) at the T_1 excited state.

Figure S8. Structural geometry of **2-5** (*left*) and **2-6** (*right*) at the T_1 excited state.

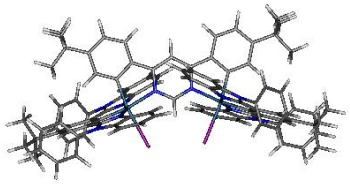

Figure S9. Structural geometry of **3-Ir2I2** at the T_1 excited state.

Figure S10. Structural geometry of **4-CNIr** (*left*) and **4-TCNIr** (*right*) at the T_1 excited state.

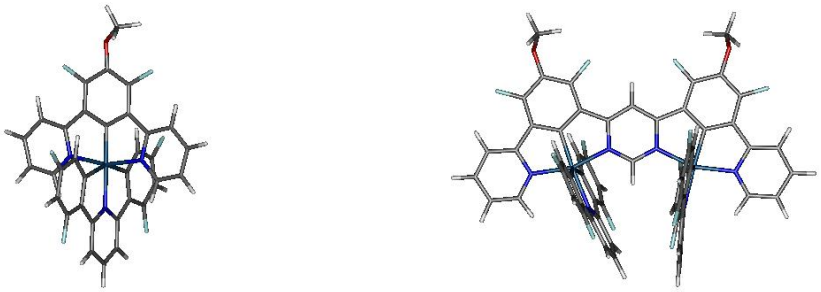

Figure S11. Structural geometry of **5-3** (*left*) and **5-5** (*right*) at the T_1 excited state.

Figure S12. Structural geometry of **6-A1** (*left*) and **6-A2** (*right*) at the T_1 excited state.

Figure S13. Structural geometry of **6-A3** (*left*) and **6-A4** (*right*) at the T_1 excited state.

Figure S14. Structural geometry of **6-A5** (*left*) and **6-B1** (*right*) at the T_1 excited state.

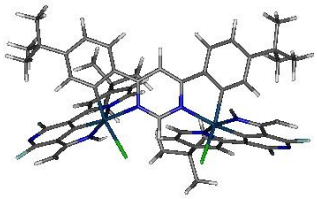

Figure S15. Structural geometry of **6-C1** at the T_1 excited state.

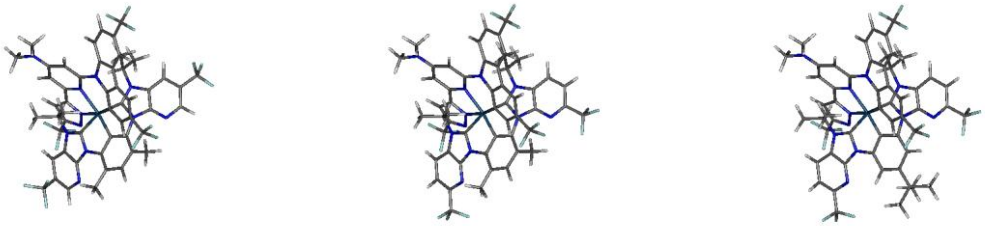

Figure S16. Structural geometry of **7-B1** (*left*), **7-B2** (*middle*), and **7-B3** (*right*) at the T_1 excited state.

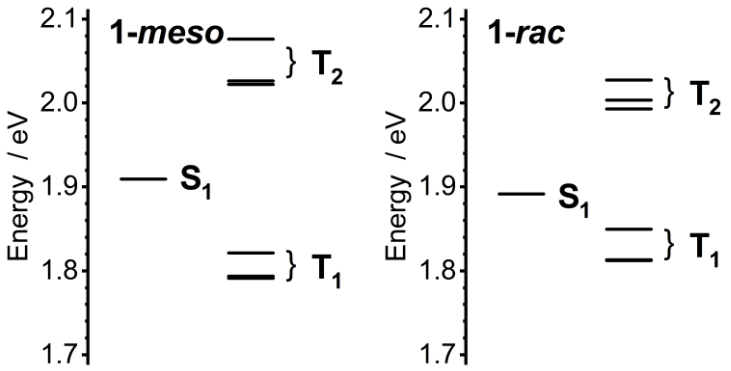

Figure S17. Excited state energy diagram for complexes **1-*meso*** and **1-*rac***.

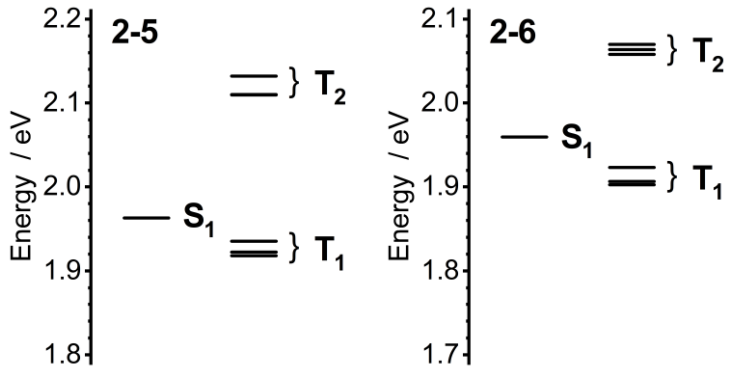

Figure S18. Excited state energy diagram for complexes **2-5** and **2-6**.

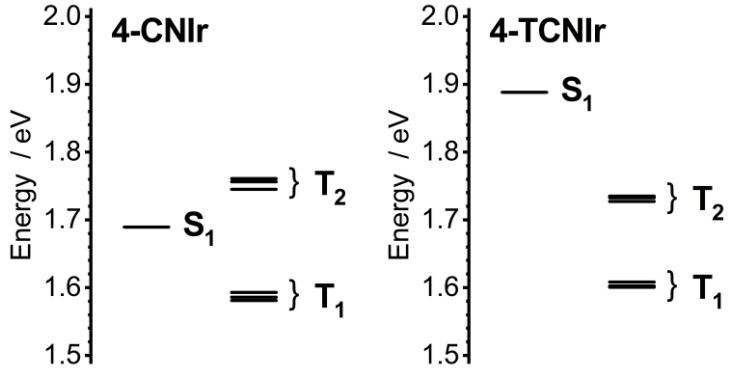

Figure S19. Excited state energy diagram for complexes **4-CNIr** and **4-TCNIr**.

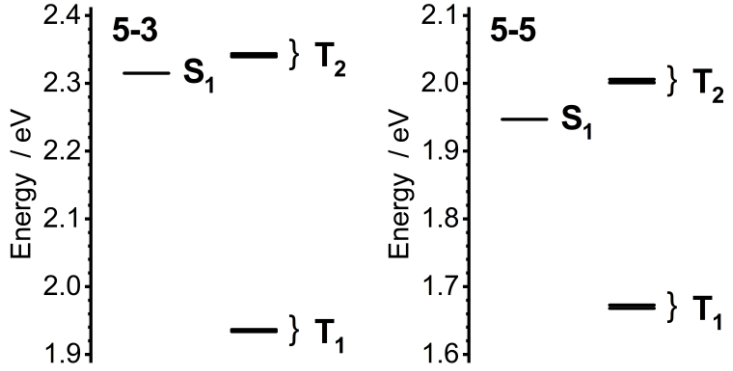

Figure S20. Excited state energy diagram for complexes **5-3** and **5-5**.

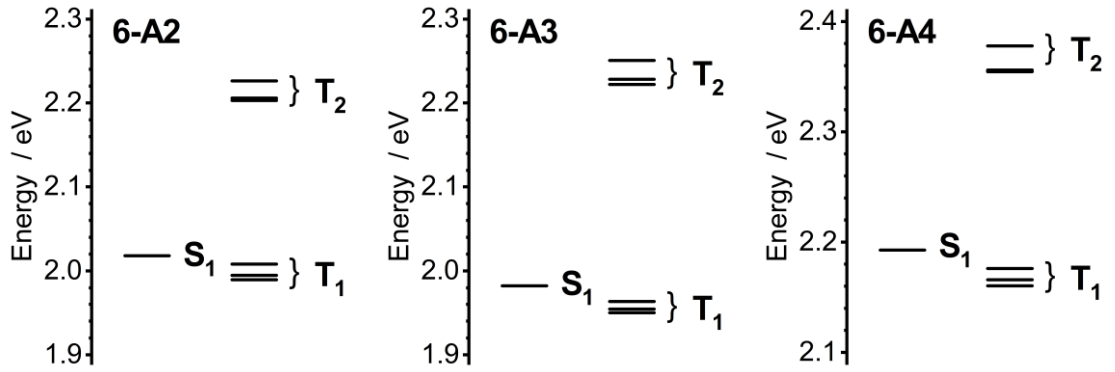

Figure S21. Excited state energy diagram for complexes **6-A2**, **6-A3** and **6-A4**.

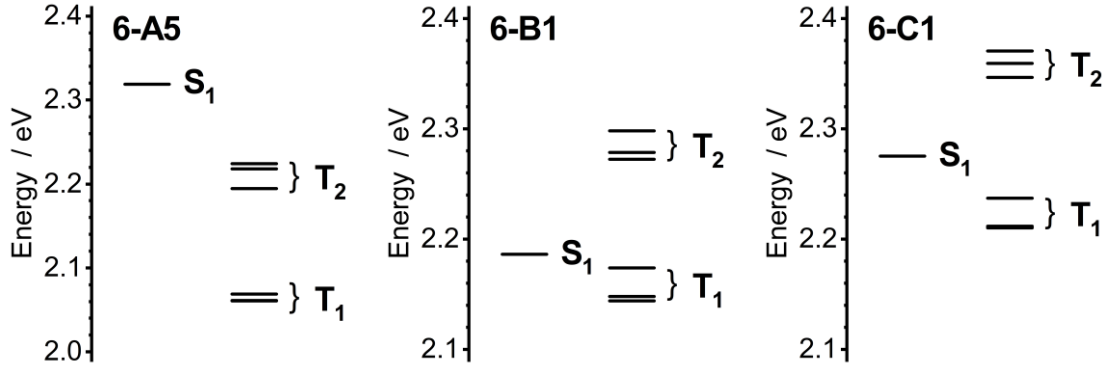

Figure S22. Excited state energy diagram for complexes **6-A5**, **6-B1** and **6-C1**.

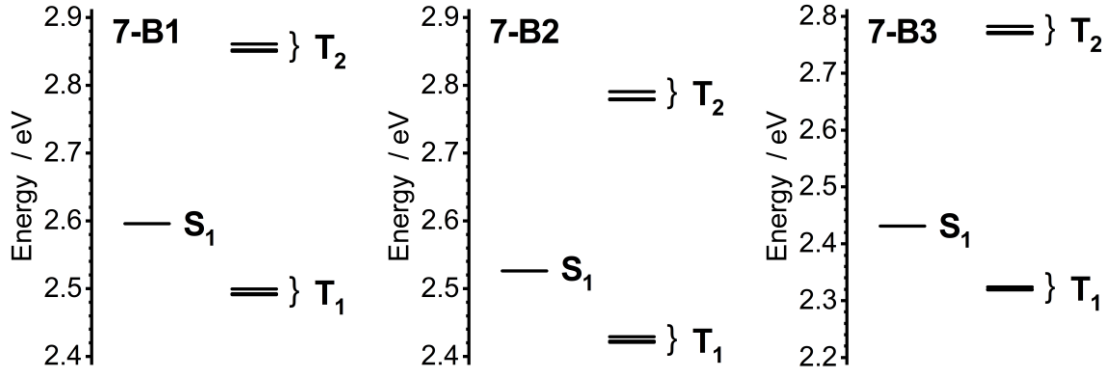

Figure S23. Excited state energy diagram for complexes **7-B1**, **7-B2** and **7-B3**.

Table S3. Calculated energy gaps between the SOC excited states in the studied iridium(III) complexes at T_1 geometry. Energy gaps equivalent to ΔE_{ST} are shown in bold font.

Complex	$\Delta E_{1\text{-}2}$, *meV*	$\Delta E_{1\text{-}3}$, *meV*	$\Delta E_{1\text{-}4}$, *meV*	$\Delta E_{1\text{-}5}$, *meV*	$\Delta E_{1\text{-}6}$, *meV*	$\Delta E_{1\text{-}7}$, *meV*
1-*rac*	1.1	37.5	**79.5**	180.6	191.2	215.0
1-*meso*	2.0	30.0	**117.8**	230.8	234.9	284.3
2-5	4.2	17.2	**45.0**	191.4	191.8	214.1
2-6	4.0	20.4	**56.8**	155.2	161.0	167.4
3-Ir_2I_2	4.4	6.8	**14.0**	283.3	287.1	309.2
4-CNIr	4.6	11.7	**108.6**	163.7	175.4	179.9
4-TCNIr	1.7	7.9	126.8	131.8	134.1	**287.7**
5-3	0.2	2.6	**380.9**	405.3	407.2	409.8
5-5	0.1	4.8	**278.3**	332.5	332.9	337.7
6-A1	5.2	17.8	**31.1**	206.0	208.3	229.6
6-A2	5.1	18.5	**28.9**	213.5	216.6	237.2
6-A3	4.4	13.3	**32.0**	271.8	278.1	300.5
6-A4	5.5	15.9	**32.5**	194.6	195.9	217.9
6-A5	0.8	8.5	134.3	157.4	163.5	**258.5**
6-B1	4.2	30.0	**42.2**	128.5	134.6	154.3
6-C1	1.4	27.0	**65.0**	136.5	149.1	160.4
7-B1	0.7	7.9	**104.6**	358.6	360.6	369.2
7-B2	1.5	7.9	**105.3**	357.6	358.9	369.4
7-B3	1.1	5.0	**112.6**	450.7	453.3	463.7

Table S4. Boltzmann probability constants between SOC states 1 and n in the studied iridium(III) complexes at T_1 geometry, at 295 K. Values associated with the occupation of the S_1 state are shown in bold font.

Complex	1-2	1-3	1-4	1-5	1-6	1-7
1-*rac*	0.959	0.229	**0.044**	0.001	0.001	0.000
1-*meso*	0.924	0.307	**0.010**	0.000	0.000	0.000
2-5	0.848	0.508	**0.170**	0.001	0.001	0.000
2-6	0.856	0.448	**0.107**	0.002	0.002	0.001
3-Ir_2I_2	0.841	0.765	**0.576**	0.000	0.000	0.000
4-CNIr	0.836	0.631	**0.014**	0.002	0.001	0.001
4-TCNIr	0.934	0.733	0.007	0.006	0.005	**0.000**
5-3	0.993	0.902	**0.000**	0.000	0.000	0.000
5-5	0.997	0.827	**0.000**	0.000	0.000	0.000
6-A1	0.814	0.496	**0.294**	0.000	0.000	0.000
6-A2	0.818	0.483	**0.321**	0.000	0.000	0.000
6-A3	0.840	0.593	**0.284**	0.000	0.000	0.000
6-A4	0.805	0.534	**0.279**	0.000	0.000	0.000
6-A5	0.971	0.717	0.005	0.002	0.002	**0.000**
6-B1	0.848	0.307	**0.190**	0.006	0.005	0.002
6-C1	0.946	0.346	**0.077**	0.005	0.003	0.002
7-B1	0.973	0.733	**0.016**	0.000	0.000	0.000
7-B2	0.941	0.733	**0.016**	0.000	0.000	0.000
7-B3	0.957	0.822	**0.012**	0.000	0.000	0.000

Table S5. Calculated cumulative radiative rates k_r^{1-n} taking into account the thermal equilibrium between the n lowest SOC states calculated for the studied iridium(III) complexes at T_1 geometry, at 295 K. k_r^{1-3} represents T_1 radiative rate. Radiative rates including the effects of both phosphorescence and TADF are shown in bold font.

Complex	k_r^{1-3}, 10^5 s^{-1}	k_r^{1-4}, 10^5 s^{-1}	k_r^{1-5}, 10^5 s^{-1}	k_r^{1-6}, 10^5 s^{-1}	k_r^{1-7}, 10^5 s^{-1}
1-*rac*	7.82	**8.44**	8.44	8.44	8.44
1-*meso*	6.00	**6.58**	6.58	6.58	6.58
2-5	16.72	**17.15**	17.15	17.14	17.14
2-6	12.39	**18.14**	18.12	18.12	18.12
3-Ir_2I_2	4.64	**4.97**	4.97	4.97	4.97
4-CNIr	5.60	**6.64**	6.64	6.64	6.64
4-TCNIr	2.89	2.92	2.95	2.95	**2.95**
5-3	0.47	**0.47**	0.47	0.47	0.47
5-5	0.46	**0.47**	0.47	0.47	0.47
6-A1	13.65	**17.83**	17.83	17.83	17.83
6-A2	12.79	**15.92**	15.92	15.91	15.91
6-A3	9.37	**13.33**	13.33	13.33	13.33
6-A4	15.28	**20.30**	20.30	20.30	20.30
6-A5	1.43	1.67	1.67	1.69	**1.69**
6-B1	7.54	**16.44**	16.40	16.40	16.42
6-C1	9.83	**14.16**	14.14	14.15	14.20
7-B1	16.35	**16.30**	16.30	16.30	16.30
7-B2	12.10	**12.14**	12.14	12.14	12.14
7-B3	8.74	**8.79**	8.79	8.79	8.79

Table S6. Composition of the seven lowest SOC states in complex **1-*rac*** at T_1 geometry.

Complex	State	Energy, eV (λ, nm)	f_{osc}	Contribution of zero-order states*
1-*rac*	1	1.8123 (684)	2.3×10^{-4}	T_1(63.2), T_2(28.7)
	2	1.8134 (684)	7.3×10^{-5}	S_5(2.3), T_1(63.2), T_2(29.2)
	3	1.8499 (670)	2.4×10^{-2}	S_1(10.0), S_3(4.9), T_1(71.5), T_2(5.0)
	4	**1.8919 (655)**	$\mathbf{1.2 \times 10^{-2}}$	**S_1(25.7), S_2(2.1), S_3(1.4), T_1(11.0), T_2(49.8)**
	5	1.9930 (620)	6.1×10^{-4}	S_1(4.4), S_2(1.4), S_9(1.6), T_1(6.6), T_2(25.7), T_3(31.9), T_4(23.3)
	6	2.0035 (619)	2.0×10^{-3}	S_1(9.4), T_1(8.1), T_2(27.2), T_3(27.4), T_4(21.3)
	7	2.0274 (612)	1.4×10^{-2}	S_1(10.8), S_2(5.9), S_3(3.1), T_1(6.7), T_2(14.2), T_3(33.9), T_4(18.8)

* States with contributions < 5% are not shown.

Table S7. Composition of the seven lowest SOC states in complex **1-*meso*** at T_1 geometry.

Complex	State	Energy, eV (λ, nm)	f_{osc}	Contribution of zero-order states*
1-*meso*	1	1.7916 (692)	3.5×10^{-4}	T_1(70.2), T_2(23.9)
	2	1.7936 (691)	1.5×10^{-4}	S_5(3.2) T_1(70.3), T_2(24.1)
	3	1.8216 (681)	1.3×10^{-2}	S_1(3.3), S_2(7.8), T_1(83.0)
	4	**1.9094 (649)**	$\mathbf{4.4 \times 10^{-2}}$	**S_1(31.0), S_2(1.9), T_2(58.5),T_6(4.0)**
	5	2.0223 (613)	2.5×10^{-4}	S_2(1.4), T_1(7.9), T_2(27.6), T_3(39.7), T_4(16.9)
	6	2.0264 (612)	1.8×10^{-3}	S_1(2,7), S_3(1.6), S_9(2.1), T_1(5.2), T_2(26.6), T_3(37.1), T_4(18.7)
	7	2.0759 (597)	2.9×10^{-2}	S_3(19.0), T_3(56.6), T_4(12.4)

* States with contributions < 5% are not shown.

Table S8. Composition of the seven lowest SOC states in complex **2-5** at T_1 geometry.

Complex	State	Energy, eV (λ, nm)	f_{osc}	Contribution of zero-order states*
2-5	1	1.9182 (646)	4.0×10^{-4}	T_1(76.0), T_3(17.4)
	2	1.9224 (645)	1.4×10^{-4}	S_2(15.4), T_1(77.8), T_5(5.3)
	3	1.9354 (641)	2.1×10^{-2}	S_7(2.3), T_1(78.5), T_3(17.1)
	4	**1.9632 (632)**	$\mathbf{6.1 \times 10^{-2}}$	**S_1(69.3), T_3(21.8), T_5(6.3)**
	5	2.1096 (588)	2.6×10^{-4}	T_2(80.2), T_4(16.1)
	6	2.1100 (588)	7.3×10^{-3}	S_9(2.5), T_2(80.6), T_4(16.1)
	7	2.1323 (582)	9.2×10^{-2}	S_4(6.4), T_2(89.9)

* States with contributions < 5% are not shown.

Table S9. Composition of the seven lowest SOC states in complex **2-6** at T_1 geometry.

Complex	State	Energy, eV (λ, nm)	f_{osc}	Contribution of zero-order states*
2-6	1	1.9027 (652)	1.6×10^{-4}	T_1(70.4), T_2(8.5), T_4(15.2)
	2	1.9066 (650)	9.9×10^{-5}	S_2(1.9), S_3(11.6), T_1(70.1), T_2(8.7)
	3	1.9231 (645)	1.7×10^{-2}	S_1(1.5), S_2(1.8), S_{14}(1.2), T_1(76.1), T_4(15.0)
	4	**1.9595 (633)**	$\mathbf{3.8 \times 10^{-2}}$	**S_1(55.3), T_2(15.3), T_4(19.5)**
	5	2.0579 (603)	6.7×10^{-4}	S_3(1.3), T_1(6.9), T_2(69.6), T_7(10.3)
	6	2.0637 (601)	2.9×10^{-3}	S_1(3.9), S_3(1.2), S_4(10.5), T_2(67.8)
	7	2.0701 (599)	3.9×10^{-3}	S_1(5.5), S_2(1.7), S_{15}(1.4), T_2(69.5), T_7(10.0)

* States with contributions < 5% are not shown.

Table S10. Composition of the seven lowest SOC states in complex **3-Ir_2I_2** at T_1 geometry.

Complex	State	Energy, eV (λ, nm)	f_{osc}	Contribution of zero-order states*
3-Ir_2I_2	1	1.6645 (745)	1.7×10^{-5}	T_1(81.0), T_3(10.6)
	2	1.6689 (743)	7.3×10^{-4}	S_1(5.7), S_4(8.7), T_1(77.0)
	3	1.6713 (742)	5.0×10^{-3}	T_1(80.4), T_3(10.5)
	4	**1.6786 (739)**	$\mathbf{2.4 \times 10^{-3}}$	**S_1(74.4), T_1(5.4), T_3(10.8)**
	5	1.9479 (637)	2.5×10^{-5}	T_2(64.7), T_3(17.5), T_8(12.9)
	6	1.9516 (635)	5.6×10^{-4}	S_6(12.2), T_2(65.7), T_3(16.2)
	7	1.9738 (628)	4.7×10^{-2}	S_1(1.1), S_4(7.5), T_2(73.8), T_8(12.4)

* States with contributions < 5% are not shown.

Table S11. Composition of the seven lowest SOC states in complex **4-CNIr** at T_1 geometry.

Complex	State	Energy, eV (λ, nm)	f_{osc}	Contribution of zero-order states*
4-CNIr	1	1.5811 (784)	7.9×10^{-6}	T_1(85.7), T_3(7.0)
	2	1.5856 (782)	3.7×10^{-3}	S_3(2.5), S_5(1.4), T_1(86.5), T_3(6.5)
	3	1.5928 (779)	5.2×10^{-3}	S_3(2.7), S_5(1.3), T_1(89.4)
	4	**1.6897** (734)	$\mathbf{7.8 \times 10^{-2}}$	**S_1(70.9), T_2(6.3), T_3(11.0)**
	5	1.7448 (711)	1.2×10^{-4}	T_2(85.3)
	6	1.7564 (706)	1.3×10^{-3}	S_1(3.7), S_4(3.9), T_2(82.8)
	7	1.7610 (704)	7.1×10^{-4}	S_6(1.9), T_2(87.3)

* States with contributions < 5% are not shown.

Table S12. Composition of the seven lowest SOC states in complex **4-TCNIr** at T_1 geometry.

Complex	State	Energy, eV (λ, nm)	f_{osc}	Contribution of zero-order states*
4-TCNIr	1	1.6007 (775)	6.0×10^{-6}	T_1(94.0)
	2	1.6024 (774)	2.9×10^{-3}	T_1(93.8)
	3	1.6086 (771)	1.0×10^{-3}	S_3(2.0), T_1(95.4)
	4	1.7275 (718)	6.3×10^{-3}	S_1(1.3), T_2(93.2)
	5	1.7325 (716)	6.1×10^{-3}	S_4(1.1), T_2(94.5)
	6	1.7348 (715)	4.9×10^{-4}	T_2(95.2)
	7	**1.8884 (657)**	**1.9×10^{-1}**	**S_1(77.1), T_3(11.9)**

Table S13. Composition of the seven lowest SOC states in complex **5-3** at T_1 geometry.

Complex	State	Energy, eV (λ, nm)	f_{osc}	Contribution of zero-order states*
5-3	1	1.9339 (641)	1.7×10^{-5}	T_1(97.8)
	2	1.9341 (641)	1.4×10^{-6}	T_1(97.8)
	3	1.9365 (640)	4.0×10^{-4}	T_1(98.4)
	4	**2.3149 (536)**	**1.8×10^{-1}**	**S_1(83.5), T_2(6.7), T_4(5.7)**
	5	2.3393 (530)	1.7×10^{-3}	S_1(1.3), T_2(90.1)
	6	2.3411 (530)	5.1×10^{-5}	S_2(1.3), T_2(95.5)
	7	2.3437 (529)	2.8×10^{-2}	S_1(6.3), S_8(1.0), T_2(86.9)

* States with contributions < 5% are not shown.

Table S14. Composition of the seven lowest SOC states in complex **5-5** at T_1 geometry.

Complex	State	Energy, eV (λ, nm)	f_{osc}	Contribution of zero-order states*
5-5	1	1.6682 (743)	8.2×10^{-7}	T_1(96.2)
	2	1.6683 (743)	3.2×10^{-5}	T_1(96.2)
	3	1.6731 (741)	5.3×10^{-4}	S_2(1.3), T_1(97.3)
	4	**1.9465 (637)**	**4.1×10^{-1}**	**S_1(84.9),T_4(6.2)**
	5	2.0007 (620)	1.3×10^{-3}	T_2(93.9)
	6	2.0011(620)	1.3×10^{-3}	T_2(93.6)
	7	2.0059(618)	3.7×10^{-3}	S_1(2.6), S_6(1.2), T_2(93.0)

* States with contributions < 5% are not shown.

Table S15. Composition of the seven lowest SOC states in complex **6-A1** at T_1 geometry.

Complex	State	Energy, eV (λ, nm)	f_{osc}	Contribution of zero-order states*
6-A1	1	2.0470 (606)	9.5×10^{-5}	T_1(78.2), T_2(10.7), T_4(5.2)
	2	2.0522 (604)	4.8×10^{-4}	S_1(5.2), S_2(1.2), S_4(1.6), T_1(75.7), T_2(9.7)
	3	2.0648 (601)	1.6×10^{-2}	S_1(10.5), S_2(4.0), S_3(1.3), T_1(74.3)
	4	**2.0781 (597)**	**1.3×10^{-2}**	**S_1(57.5), T_1(15.7), T_2(13.4), T_4(6.1)**
	5	2.2530 (550)	1.3×10^{-4}	S_1(2.8), T_2(47.6), T_4(16.2), T_5(18.5)
	6	2.2553 (550)	3.6×10^{-4}	S_2(3.1), S_3(12.7), T_1(6.3), T_2(49.0), T_4(18.1)
	7	2.2766 (545)	5.2×10^{-3}	S_1(5.1), S_3(1.6), S_4(3.1), S_{10}(1.1), S_{11}(1.4), T_2(50.6), T_4(12.9), T_5(18.1)

* States with contributions < 5% are not shown.

Table S16. Composition of the seven lowest SOC states in complex **6-A2** at T_1 geometry.

Complex	State	Energy, eV (λ, nm)	f_{osc}	Contribution of zero-order states*
6-A2	1	1.9894 (623)	9.4×10^{-5}	T_1(79.3), T_2(10.4)
	2	1.9946 (622)	4.6×10^{-4}	S_1(4.9), S_2(1.1), S_4(1.6), T_1(76.9), T_2(9.4)
	3	2.0080 (618)	1.6×10^{-2}	S_1(8.4), S_2(3.7), S_3(1.2), T_1(77.5)
	4	**2.0183 (614)**	**1.1×10^{-2}**	**S_1(61.7), T_1(13.2), T_2(12.9), T_3(5.7)**
	5	2.2029 (563)	8.2×10^{-5}	S_1(2.5), T_2(45.4), T_3(19.7), T_5(19.6)
	6	2.2060 (562)	2.8×10^{-4}	S_2(3.3), S_3(12.6), T_1(5.6), T_2(46.9), T_3(20.1)
	7	2.2266 (557)	5.7×10^{-3}	S_1(4.4), S_3(2.0), S_4(3.6), S_{10}(1.8), T_2(48.6), T_3(14.9), T_5(18.5)

* States with contributions < 5% are not shown.

Table S17. Composition of the seven lowest SOC states in complex **6-A3** at T_1 geometry.

Complex	State	Energy, eV (λ, nm)	f_{osc}	Contribution of zero-order states*
6-A3	1	1.9502 (636)	7.1×10^{-5}	T_1(84.9), T_2(5.2)
	2	1.9547 (634)	1.8×10^{-4}	S_1(2.5), S_3(1.6), T_1(84.3), T_2(5.6)
	3	1.9635 (632)	1.1×10^{-2}	S_1(12.0), S_2(1.2), S_3(2.2), T_1(76.8)
	4	**1.9822 (626)**	**1.4×10^{-2}**	**S_1(67.9), T_1(15.4), T_2(8.2)**
	5	2.2220 (558)	4.2×10^{-5}	S_1(1.6), T_2(36.0), T_3(22.8), T_5(26.1), T_7(5.0)
	6	2.2283 (556)	2.6×10^{-4}	S_2(12.3), S_3(9.6), T_2(37.2), T_3(23.7)
	7	2.2507 (551)	5.3×10^{-3}	S_1(2.2), S_4(7.7), S_9(1.6), T_2(41.4), T_3(12.6), T_5(25.7)

* States with contributions < 5% are not shown.

Table S18. Composition of the seven lowest SOC states in complex **6-A4** at T_1 geometry.

Complex	State	Energy, eV (λ, nm)	f_{osc}	Contribution of zero-order states*
6-A4	1	2.1601 (574)	9.0×10^{-5}	T_1(77.3), T_3(5.9), T_4(5.0)
	2	2.1657 (573)	4.5×10^{-4}	S_1(6.6), S_2(1.6), S_4(1.9), T_1(74.0), T_3(5.5)
	3	2.1761 (570)	1.5×10^{-2}	S_1(11.7), S_2(3.7), T_1(72.1), T_4(5.0)
	4	**2.1926 (566)**	**1.5×10^{-2}**	**S_1(52.8), T_1(19.2), T_2(6.6), T_3(6.8), T_4(6.4)**
	5	2.3548 (527)	5.3×10^{-5}	S_1(3.4), T_1(5.3), T_2(28.8), T_3(26.0), T_4(13.7), T_6(11.1)
	6	2.3560 (526)	3.7×10^{-4}	S_2(1.7), S_3(9.0), T_1(8.7), T_2(31.6), T_3(25.3), T_4(14.0)
	7	2.3781 (521)	2.0×10^{-3}	S_1(4.5), T_2(51.5), T_3(26.6)

* States with contributions < 5% are not shown.

Table S19. Composition of the seven lowest SOC states in complex **6-A5** at T_1 geometry.

Complex	State	Energy, eV (λ, nm)	f_{osc}	Contribution of zero-order states*
6-A5	1	2.0605 (602)	1.2×10^{-4}	T_1(84.2), T_2(7.7)
	2	2.0613 (602)	6.9×10^{-4}	S_1(3.7), T_1(84.7), T_2(7.0)
	3	2.0690 (599)	3.3×10^{-4}	T_1(90.5)
	4	2.1948 (565)	3.1×10^{-2}	S_2(2.8), S_3(1.1), T_2(82.5), T_3(7.4)
	5	2.2179 (559)	4.0×10^{-4}	T_1(9.4), T_2(78.6)
	6	2.2240 (558)	6.8×10^{-3}	S_1(1.8), T_1(9.5), T_2(81.0)
	7	**2.3190 (535)**	**3.0×10^{-2}**	**S_1(50.6), S_2(3.2), T_3(27.9)**

* States with contributions < 5% are not shown.

Table S20. Composition of the seven lowest SOC states in complex **6-B1** at T_1 geometry.

Complex	State	Energy, eV (λ, nm)	f_{osc}	Contribution of zero-order states*
6-B1	1	2.1439 (578)	3.6×10^{-4}	T_1(59.0), T_2(21.0), T_3(12.1)
	2	2.1481 (577)	3.3×10^{-4}	S_1(9.4), S_2(2.9), S_3(1.5), S_4(2.1), T_1(55.2), T_2(19.9)
	3	2.1739 (570)	1.1×10^{-2}	S_1(15.4), S_8(1.1), T_1(45.8), T_2(16.8), T_3(15.3)
	4	**2.1861 (567)**	**2.8×10^{-2}**	**S_1(17.0), S_2(6.7), S_4(3.4), T_1(33.7), T_2(22.2), T_3(8.8)**
	5	2.2724 (546)	5.4×10^{-4}	S_1(3.9), T_1(9.9), T_2(49.1), T_3(10.7), T_4(10.5)
	6	2.2785 (544)	3.1×10^{-3}	S_2(2.7), S_3(7.4), S_4(3.1), T_1(14.4), T_2(49.4), T_3(8.2), T_4(5.2)
	7	2.2982 (540)	9.0×10^{-3}	S_1(13.6), S_3(3.5), S_9(2.2), T_2(38.7), T_3(19.5), T_4(13.8)

* States with contributions < 5% are not shown.

Table S21. Composition of the seven lowest SOC states in complex **6-C1** at T_1 geometry.

Complex	State	Energy, eV (λ, nm)	f_{osc}	Contribution of zero-order states*
6-C1	1	2.2102 (561)	5.9×10^{-4}	T_1(68.9), T_2(15.2), T_3(8.2)
	2	2.2116 (561)	1.6×10^{-4}	S_3(7.3), T_1(67.6), T_2(17.5)
	3	2.2372 (554)	1.3×10^{-2}	S_1(1.9), S_2(1.9), T_1(81.1), T_3(8.5)
	4	**2.2752 (545)**	**3.1×10^{-2}**	**S_1(34.1), S_4(1.3), T_2(46.1), T_3(7.6), T_4(5.7)**
	5	2.3467 (528)	9.7×10^{-4}	S_1(1.1), S_3(1.1), S_4(2.1), T_1(12.9), T_2(64.2)
	6	2.3593 (526)	4.3×10^{-3}	S_1(2.8), S_{10}(1.2), T_1(12.0), T_2(67.7), T_6(5.4)
	7	2.3706 (523)	1.8×10^{-2}	S_1(26.2), S_4(3.0), T_2(39.0), T_3(15.3)

* States with contributions < 5% are not shown.

Table S22. Composition of the seven lowest SOC states in complex **7-B1** at T_1 geometry.

Complex	State	Energy, eV (λ, nm)	f_{osc}	Contribution of zero-order states*
7-B1	1	2.4915 (498)	4.6×10^{-5}	S_2(1.2), S_4(1.3), T_1(90.4)
	2	2.4922 (498)	1.3×10^{-6}	T_1(89.9), T_2(6.2)
	3	2.4994 (496)	1.1×10^{-2}	S_2(2.5), T_1(93.1)
	4	**2.5961 (478)**	**1.4×10^{-3}**	**S_1(81.2), T_2(9.5)**
	5	2.8501 (435)	3.7×10^{-5}	T_1(7.2), T_2(81.7), T_4(5.4)
	6	2.8521 (435)	5.9×10^{-4}	S_2(1.2), S_4(2.5), T_1(6.9), T_2(83.7)
	7	2.8608 (433)	8.8×10^{-4}	S_1(12.8), T_2(78.5)

* States with contributions < 5% are not shown.

Table S23. Composition of the seven lowest SOC states in complex **7-B2** at T_1 geometry.

Complex	State	Energy, eV (λ, nm)	f_{osc}	Contribution of zero-order states*
7-B2	1	2.4211 (512)	9.9×10^{-6}	S_4(1.4), T_1(91.1)
	2	2.4226 (512)	1.4×10^{-6}	T_1(90.9), T_2(5.5)
	3	2.4290 (510)	8.5×10^{-3}	S_2(2.6), T_1(93.8)
	4	**2.5264 (491)**	**3.1×10^{-3}**	**S_1(81.3), T_2(10.6)**
	5	2.7787 (446)	6.0×10^{-5}	T_1(6.9), T_2(84.5)
	6	2.7799 (446)	2.6×10^{-4}	S_4(2.5), T_1(7.3), T_2(86.2)
	7	2.7905 (444)	1.4×10^{-3}	S_1(13.0), T_2(80.9)

* States with contributions < 5% are not shown.

Table S24. Composition of the seven lowest SOC states in complex **7-B3** at T_1 geometry.

Complex	State	Energy, eV (λ, nm)	f_{osc}	Contribution of zero-order states*
7-B3	1	2.3188 (535)	1.8×10^{-5}	T_1(94.4)
	2	2.3199 (535)	6.9×10^{-6}	T_1(94.2)
	3	2.3238 (534)	6.2×10^{-3}	S_2(1.5), T_1(95.6)
	4	**2.4314 (510)**	**3.7×10^{-3}**	**S_1(90.0)**
	5	2.7695 (448)	2.2×10^{-5}	T_2(68.3), T_3(17.8)
	6	2.7721 (447)	4.2×10^{-4}	S_2(1.0), S_4(2.2), T_2(69.2), T_3(19.0)
	7	2.7825 (446)	4.4×10^{-3}	S_1(4.6), T_2(80.6), T_3(5.3), T_4(5.8)

* States with contributions < 5% are not shown.

Table S25. Orbital pairing of the S_1 and T_1 TD-DFT states. H – HOMO; L – LUMO.

Complex	Orbital pairing		State	
	S_1	T_1	S_1	T_1
1-*rac*	H→L (94%)	H→L (90%)	$d_{Ir\text{-}1} + p_{Cl\text{-}1} + \pi_{L1} \rightarrow \pi_{L2}^*$	$d_{Ir\text{-}1} + p_{Cl\text{-}1} + \pi_{L1} \rightarrow \pi_{L2}^*$
1-*meso*	H→L (88%)	H→L (93%)	$d_{Ir\text{-}1} + p_{Cl\text{-}1} + \pi_{L1} \rightarrow \pi_{L2}^*$	$d_{Ir\text{-}1} + p_{Cl\text{-}1} + \pi_{L1} \rightarrow \pi_{L2}^*$
2-5	H→L (99%)	H→L (96%)	$d_{Ir} + p_{Cl} + \pi_{L1} \rightarrow \pi_{L2}^*$	$d_{Ir} + p_{Cl} + \pi_{L1} \rightarrow \pi_{L2}^*$
2-6	H→L (98%)	H→L (96%)	$d_{Ir\text{-}1} + p_{Cl\text{-}1} + \pi_{L1} \rightarrow \pi_{L2}^*$	$d_{Ir1} + p_{Cl\text{-}1} + \pi_{L1} \rightarrow \pi_{L2}^*$
3-Ir_2I_2	H→L (99%)	H→L (99%)	$d_{Ir\text{-}1,2} + p_{I\text{-}1,2} + \pi_{L1} \rightarrow \pi_{L2}^*$	$d_{Ir1,2} + p_{I\text{-}1,2} + \pi_{L1} \rightarrow \pi_{L2}^*$
4-CNIr	H→L (98%)	H→L (94%)	$d_{Ir} + \pi_{Ph} \rightarrow \pi_{iquin}^*$	$d_{Ir} + \pi_{Ph} \rightarrow \pi_{iquin}^*$
4-TCNIr	H→L (97%)	H→L (89%)	$d_{Ir} + \pi_{Th} \rightarrow \pi_{iquin}^*$	$d_{Ir} + \pi_{Th} \rightarrow \pi_{iquin}^*$
5-3	H→L (97%)	H→L (98%)	$d_{Ir} + \pi_{L1} \rightarrow \pi_{L1}^*$	$d_{Ir} + \pi_{L1} \rightarrow \pi_{L1}^*$
5-5	H→L (94%)	H→L (97%)	$d_{Ir\text{-}1,2} + \pi_{L1} \rightarrow \pi_{L1}^*$	$d_{Ir\text{-}1,2} + \pi_{L1} \rightarrow \pi_{L1}^*$
6-A1	H→L (98%)	H→L (96%)	$d_{Ir\text{-}1} + p_{Cl\text{-}1} + \pi_{L2} \rightarrow \pi_{L1}^*$	$d_{Ir\text{-}1} + p_{Cl\text{-}1} + \pi_{L2} \rightarrow \pi_{L1}^*$
6-A2	H→L (98%)	H→L (97%)	$d_{Ir\text{-}1} + p_{Cl\text{-}1} + \pi_{L2} \rightarrow \pi_{L1}^*$	$d_{Ir\text{-}1} + p_{Cl\text{-}1} + \pi_{L2} \rightarrow \pi_{L1}^*$
6-A3	H→L (98%)	H→L (97%)	$d_{Ir\text{-}1} + p_{Cl\text{-}1} + \pi_{L2} \rightarrow \pi_{L1}^*$	$d_{Ir\text{-}1} + p_{Cl\text{-}1} + \pi_{L2} \rightarrow \pi_{L1}^*$
6-A4	H→L (98%)	H→L (95%)	$d_{Ir\text{-}1} + p_{Cl\text{-}1} + \pi_{L2} \rightarrow \pi_{L1}^*$	$d_{Ir\text{-}1} + p_{Cl\text{-}1} + \pi_{L2} \rightarrow \pi_{L1}^*$
6-A5	H→L (97%)	H-1→L (83%)	$d_{Ir\text{-}1} + p_{Cl\text{-}1} + \pi_{L2} \rightarrow \pi_{L1}^*$	$d_{Ir\text{-}1} + p_{Cl\text{-}1} + \pi_{L1} \rightarrow \pi_{L1}^*$
6-B1	H→L (98%)	H→L (85%)	$d_{Ir\text{-}1} + p_{Cl\text{-}1} + \pi_{L2} \rightarrow \pi_{L1}^*$	$d_{Ir\text{-}1} + p_{Cl\text{-}1} + \pi_{L2} \rightarrow \pi_{L1}^*$
6-C1	H→L (98%)	H→L (92%)	$d_{Ir\text{-}1} + p_{Cl\text{-}1} + \pi_{L2} \rightarrow \pi_{L1}^*$	$d_{Ir\text{-}1} + p_{Cl\text{-}1} + \pi_{L2} \rightarrow \pi_{L1}^*$
7-B1	H→L (98%)	H→L (92%)	$d_{Ir} + \pi_{L1} \rightarrow \pi_{L1}^*$	$d_{Ir} + \pi_{L1} \rightarrow \pi_{L1}^*$
7-B2	H→L (98%)	H→L (93%)	$d_{Ir} + \pi_{L1} \rightarrow \pi_{L1}^*$	$d_{Ir} + \pi_{L1} \rightarrow \pi_{L1}^*$
7-B3	H→L (99%)	H→L (95%)	$d_{Ir} + \pi_{L1} \rightarrow \pi_{L1}^*$	$d_{Ir} + \pi_{L1} \rightarrow \pi_{L1}^*$

* Transitions with contribution < 10% are not shown.

Table S26. HOMO and LUMO energy and energy gaps at the T_1 geometry.

Complex	Energy, eV		E_g, eV
	HOMO	LUMO	
1-*rac*	-5.4453	-2.7596	2.6857
1-*meso*	-5.4220	-2.7522	2.6698
2-5	-4.8744	-2.1936	2.6808
2-6	-4.8337	-2.1182	2.7155
3-Ir_2I_2	-4.5632	-2.1637	2.3995
4-CNIr	-5.3631	-2.9169	2.4462
4-TCNIr	-5.3645	-2.8222	2.5423
5-3	-4.9704	-2.0754	2.8950
5-5	-5.1006	-2.6100	2.4906
6-A1	-5.1248	-2.4014	2.7234
6-A2	-5.1517	-2.4914	2.6603
6-A3	-5.2305	-2.6298	2.6007
6-A4	-5.1297	-2.2998	2.8299
6-A5	-5.2454	-2.2744	2.9710
6-B1	-5.3746	-2.4153	2.9593
6-C1	-5.5642	-2.5016	3.0626
7-B1	-5.3876	-2.1530	3.2346
7-B2	-5.3620	-2.2082	3.1538
7-B3	-5.3048	-2.2628	3.0420

Table S27. Spin-orbit coupling matrix elements between S_1 and T_1 states, $\langle T_1 | \hat{H}_{SO} | S_1 \rangle$, at the T_1 geometry.

Complex	$\langle \mathbf{T_1} \vert \hat{H}_{\mathbf{SO}} \vert \mathbf{S_1} \rangle$**, cm^{-1}**
1-*rac*	272.4
1-*meso*	315.8
2-5	24.6
2-6	85.9
3-Ir_2I_2	47.8
4-CNIr	56.5
4-TCNIr	42.0
5-3	2.7
5-5	82.4
6-A1	58.9
6-A2	48.7
6-A3	56.7
6-A4	72.2
6-A5	446.4
6-B1	227.3
6-C1	143.5
7-B1	11.5
7-B2	13.3
7-B3	21.7

4. OLEDs

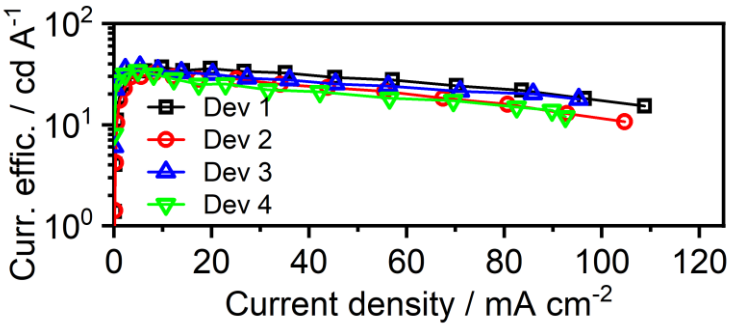

Figure S24. Current efficiency as a function of current density in devices 1-4.

Table S28. Characteristics of OLED devices 1-6 using **6** as the emitter.

	Dev 1	**Dev 2**	**Dev 3**	**Dev 4**
Emitter	**6-A1**	**6-A1**	**6-A1**	**6-A1**
V_{ON} / V [a]	6.0	6.0	6.8	5.7
L_{max} / mW cm^{-2} [b]	18 400	12 900	17 300	12 500
λ_{EL} / nm [c]	545	539	551	549
CE_{max} / cd A^{-1} [d]	37.1	32.5	37.4	34.2
EQE_{max} / % [e]	9.5	8.4	9.7	8.8
EQE_{mean} / % [f]	9.4	8.1	9.1	8.5
EQE_{median} / % [g]	9.4	8.1	9.2	8.8

[a] turn-on voltage at 1 cd m^{-2}; [b] maximum luminance; [c] electroluminescence spectrum maxima; [d] current efficiency; [e] maximum external quantum efficiency; [f] mean external quantum efficiency over 8 pixels; [g] median external quantum efficiency over 8 pixels.

Table S29. OLED architecture for devices 1-6 presented in the main article.

Device	**Architecture**
Dev 1	ITO | AI4083 (30 nm) | PVKH (10) | mCP:PO-T2T (70:30) co. **6-A1** (3%) (~30 nm) | PO-T2T (50 nm) | LiF (0.8 nm) | Al (100 nm)
Dev 2	ITO | AI4083 (30 nm) | PVKH (10) | mCP:PO-T2T (70:30) co. **6-A1** (1%) (~30 nm) | PO-T2T (50 nm) | LiF (0.8 nm) | Al (100 nm)
Dev 3	ITO | AI4083 (30 nm) | PVKH (10) | mCP:PBD (60:40) co. **6-A1** (3%) (~30 nm) | TmPyPB (50 nm) | LiF (0.8 nm) | Al (100 nm)
Dev 4	ITO | AI4083 (30 nm) | PVKH (10) | mCP:PBD (60:40) co. **6-A1** (1%) (~30 nm) | TmPyPB (50 nm) | LiF (0.8 nm) | Al (100 nm)

5. References

[1] F. Neese, *WIREs Comput. Mol. Sci.* **2018**, *8*, DOI: 10.1002/wcms.1327.

[2] F. Neese, *WIREs Comput. Mol. Sci.* **2012**, *2*, 73.

[3] S. Lehtola, C. Steigemann, M. J. T. Oliveira, M. A. L. Marques, *SoftwareX* **2018**, *7*, 1.

[4] A.-R. Allouche, *J. Comput. Chem.* **2011**, *32*, 174.

[5] A. D. Becke, *J. Chem. Phys.* **1993**, *98*, 5648.

[6] P. J. Stephens, F. J. Devlin, C. F. Chabalowski, M. J. Frisch, *J. Phys. Chem.* **1994**, *98*, 11623.

[7] F. Weigend, R. Ahlrichs, *Phys. Chem. Chem. Phys.* **2005**, *7*, 3297.

[8] F. Weigend, *Phys. Chem. Chem. Phys.* **2006**, *8*, 1057.

[9] E. van Lenthe, E. J. Baerends, J. G. Snijders, *J. Chem. Phys.* **1993**, *99*, 4597.

[10] E. van Lenthe, E. J. Baerends, J. G. Snijders, *J. Chem. Phys.* **1994**, *101*, 9783.

[11] D. A. Pantazis, X. Y. Chen, C. R. Landis, F. Neese, *J. Chem. Theory Comput.* **2008**, *4*, 908.

[12] F. Neese, F. Wennmohs, A. Hansen, U. Becker, *Chem. Phys.* **2009**, *356*, 98.

[13] R. Izsák, F. Neese, *J. Chem. Phys.* **2011**, *135*, 144105.

[14] K. Nozaki, *J. Chinese Chem. Soc.* **2006**, *53*, 101.

[15] K. Mori, T. P. M. Goumans, E. van Lenthe, F. Wang, *Phys. Chem. Chem. Phys.* **2014**, *16*, 14523.

[16] P. Data, P. Pander, M. Lapkowski, A. Swist, J. Soloducho, R. R. Reghu, J. V. Grazulevicius, *Electrochim. Acta* **2014**, *128*, 430.

[17] P. Pander, P. Data, R. Turczyn, M. Lapkowski, A. Swist, J. Soloducho, A. P. Monkman, *Electrochim. Acta* **2016**, *210*, 773.

[18] C. M. Cardona, W. Li, A. E. Kaifer, D. Stockdale, G. C. Bazan, *Adv. Mater.* **2011**, *23*, 2367.

[19] J.-L. Bredas, *Mater. Horiz.* **2014**, *1*, 17.

[20] P. Pander, P. Data, F. B. Dias, *J. Vis. Exp.* **2018**, DOI: 10.3791/56614.

[21] D. de Sa Pereira, A. P. Monkman, P. Data, *J. Vis. Exp.* **2018**, DOI: 10.3791/56593.

[22] P. Pander, A. V. Zaytsev, A. Sil, J. A. G. Williams, P.-H. Lanoe, V. N. Kozhevnikov, F. B. Dias, *J. Mater. Chem. C* **2021**, *9*, 10276.

[23] O. V. Dolomanov, L. J. Bourhis, R. J. Gildea, J. A. K. Howard, H. Puschmann, *J. Appl. Crystallogr.* **2009**, *42*, 339.